Materials Science and Engineering A 403 (2005) 134–143

MATERIALS SCIENCE & ENGINEERING A

www.elsevier.com/locate/msea

Mechanical behavior of tungsten preform reinforced bulk metallic glass composites

Hao Li [a], Ghatu Subhash [a,*], Laszlo J. Kecskes [b], Robert J. Dowding [b]

[a] *Department of Mechanical Engineering–Engineering Mechanics, Michigan Technological University, 1400 Townsend Drive, Houghton, MI 49931, USA*

[b] *Weapons and Materials Research Directorate, US Army Research Laboratory, Aberdeen Proving Ground, MD 21005, USA*

Accepted 25 April 2005

Abstract

Quasistatic and dynamic compression tests were conducted on four tungsten preform reinforced Vit105 ($Zr_{52.5}Ti_5Cu_{17.9}Ni_{14.6}Al_{10}$) and Vit106 ($Zr_{57}Nb_5Cu_{15.4}Ni_{12.6}Al_{10}$) metallic glass composites. All the composites exhibited large plastic strain under both quasistatic and dynamic compression. In general, the dynamic loading resulted in higher failure stress than the quasistatic loading. The deformation behavior was found to be dominated by the ductile W phase. Microscopic observation of the deformed and fractured specimens revealed shear banding in the glassy phase, cracking along the particle boundaries and severe deformation of W particles. It is also found that the processing methods have strong influence on the mechanical behavior of the composites even when they have the same matrix and the same volume fractions of the reinforcement.

Keywords: Metallic glass matrix composite; Compression behavior; Hopkinson pressure bar; Shear band; Tungsten preform

1. Introduction

Vit105 ($Zr_{52.5}Ti_5Cu_{17.9}Ni_{14.6}Al_{10}$) and Vit106 ($Zr_{57}Nb_5Cu_{15.4}Ni_{12.6}Al_{10}$) are among the best glass formers developed in recent years [1]. However, like most other metallic glasses, they fail catastrophically under quasistatic compressive loads due to the formation of shear bands. Various methods have been adopted to enhance the toughness of metallic glasses. They are (i) partial devitrification of as-cast metallic glass [2,3], (ii) in-situ precipitation of a dendritic metallic phase from the melt during casting [4,5], (iii) addition of crystalline particles to the melt prior to casting [6], (iv) casting a glass-forming liquid around particles/fibers of a second phase [7], and (v) mechanical alloying of elemental powders blended with insoluble particles [8–11]. There is no apparent advantage of one processing method over the other among the above approaches in terms of resulting mechanical properties. However, the annealing method is supposed to cause brittleness to the material because of structural relaxation or precipitation of crystalline phase from the amorphous matrix during the process [12].

Because Vit105 and Vit106 are both good glass formers, they can be used as matrix materials. The advantages include their relatively low melting temperatures and the low glass transition temperatures. The former slows the chemical interaction between the reinforcement and the glass, and the latter reduces the differential thermal stresses thus leading to less stress concentration during freezing and cooling.

Numerous composites have been produced using Vit105 or Vit106 metallic glasses. They have been reinforced with refractory ceramic particles and ductile metal particles or short fibers [13]. It was found that although Vit105 has better glass forming ability (GFA) than Vit106 [14], the latter has better process stability to maintain its full glass matrix state in the composites [13]. Extensive investigations on Vit106 matrix composites were initiated by Johnson and co-workers in the late 1990s. They introduced various refractory ceramic particles (SiC, TiC, and WC), ductile metals particles (W, Ta, Nb, Mo, and W/Re), and W wires or fibers into the Vit106

* Corresponding author. Tel.: +1 906 487 3161; fax: +1 906 487 2822.
E-mail address: subhash@mtu.edu (G. Subhash).

0921-5093/$ – see front matter © 2005 Elsevier B.V. All rights reserved.
doi:10.1016/j.msea.2005.04.053

matrix with a range of dimensions and volume fractions [6,13,15–19]. It was found that the addition of the second phase crystalline materials into Vit106 (as well as Vit105 and Vit101) does not significantly degrade the GFA of the matrix alloy [6,13].

The mechanical behavior of the above composites has also been well investigated under a variety of loading conditions [2,16,17,20,21]. Vit106 composite reinforced with 15% particulate W of size 150 μm exhibited an increased compressive strain by up to 300% under quasistatic compression [15,17]. A composite of Vit106 with W fiber reinforcement fail by localized fiber buckling and tilting in compression but the failure strain increased dramatically. With 80% W wire (diameter 254 μm) reinforcement, the compressive strain reached 16.2% (while the pure glass Vit106 has only 0.5% inelastic strain and 2% elastic strain) [17]. Compressive strength increased with both W wire and W or W/Re particulate additions [17]. The addition of low volume fraction (10%) of Nb, Ta, and Mo particles (2–3 μm) does not significantly enhance the plasticity and strength of the composite. However, higher volume fractions (50%) of larger particles (30–200 μm) of the above metals increased the failure strains dramatically from 6 to 24%, but reduced the yield stress and compressive strength [19]. The W particulate composites, with large volume fraction (up to 50%) and small size particles, failed similar to ductile materials in tension [16]. The tensile fracture toughness was also increased by more than 50% with the ductile W or Ta particles due to their ability to obstruct shear banding and increase fracture surface in the composite [15]. A metallic glass composite reinforced by tungsten preform has been reported to exhibit large plastic strain in excess of 30% [21].

In general, reinforcement in the form of particle, wire or fiber into Vit106 glass matrix enhances failure strain and fracture toughness of the composite but not necessarily the strength. The fracture mode for particle reinforced composite is similar to that for the glass (i.e., approximately 45° fracture angle), while for aligned fiber reinforced composite, the specimens fail by wire splitting, buckling, and tilting in compression.

Bian et al. [22] studied the shear band patterns on the fracture surface of annealed Vit105 in which uniformly distributed nanocrystals were produced by heat treatment. It was found that shear bands become thinner and denser with increase in nanocrystal volume fraction, and when the volume fraction reaches a critical value (42%), no shear bands can be observed on the fracture surfaces of quasistatically compressed specimens. However, these intermetallic nanoparticles caused embrittlement of the materials. Vit105 was recently reinforced with carbon-nanotubes (CNT) by the conventional die cast method [23]. It was found that the elastic moduli and the ultrasonic absorption ability of the composite increased while the density decreased [24].

In summary, Vit105 and Vit106 have been reinforced with various ductile or brittle materials, as well as carbon-nanobubes, by diverse processing methods. The resulting composites have improved plastic strain. In this paper, the elastic properties, the constitutive behavior, and the fracture modes of a new class of metallic glass matrix composites is studied. The composite was made by infiltrating melt glass into a W preform as described in detail in the next section.

2. Materials and experimental procedure

Four tungsten preform reinforced metallic glass matrix composites, namely, Vit106-W60, Vit106(LM)-W60, Vit106(LM)-W70, and Vit105-W70, were used in this investigation. In the above composites, either Vit106 or Vit105 was used as the glass matrix, and tungsten (W) at either 60 or 70% (v/v) was used as reinforcement. All the W preforms except those for Vit106-W60 were made at SpectraMat, Inc., Watsonville, CA, and the preforms for Vit106-W60 were made at the US Army Research Laboratory, Aberdeen Proving Ground, MD. The infiltration of metallic glass was performed at Liquidmetal (LM) Technologies, Lake Forest, CA. For Vit106(LM)-W60 and Vit106(LM)-W70, yttrium was used in the glass melt to remove oxygen at LM, and the Vit106 is thus denoted as Vit106(LM).

The procedure for making the W preforms at SpectraMat is as follows. The W powder was cold isostatically pressed (CIP) into a porous block at 18,000 psi. The block was cut into rods and sintered at above 2000 °C in hydrogen (to diminish surface oxidation). The rods were infiltrated with methyl methacrylate, and the resulting poly methyl methacrylate (PMMA) was cured and machined to desired dimensions. The PMMA was then burned out in hydrogen fire at 1500 °C to clean up the preform. The W preforms for Vit106-W60 were made in a similar way, with pressure at 30,000 psi for CIPping and temperature at 900 °C for sintering. For the W preform for Vit105-W70, an extra foaming procedure was used. The fine W powders were mixed with a fugitive agent so that when the powders were pressed and sintered, a sponge-like material with bimodal pore structure was created. The large pores resulted from burning of large chunks of fugitive agent and the small porous structure from the normally sintered and pressed W powders. The infiltration for all the four composites was conducted at LM and the process typically involved three steps. First, preheating the preform and the glass in a vacuumed stainless steel tube to a temperature above the liquidus of the Vit106 and Vit105; second, forcing the viscous liquid into the preform by applying argon gas pressure allowing the infiltration to proceed; finally, the tube was removed from the furnace and quenched in water.

The as received 8-mm diameter composite rods were electric discharge machined (EDM) to small prisms with a side dimension of ∼2.44 mm and a length ∼4.51 mm. The prismatic shape was chosen for the convenience of being able to polish the side surfaces for postmortem scanning electron microscope (SEM) observations. The specimen surfaces were ground and polished to obtain orthogonality of the prismatic sides. X-ray diffraction (XRD) and dif-

ferential scanning calorimetry (DSC) examinations were later conducted to verify that the matrices were mostly of amorphous structure. The density and the elastic properties of the composites were measured using Archimedes principle and ultrasonic wave velocities, respectively. These properties were also calculated using the rule of mixture (ROM).

At least three specimens from each composite were compressed on a servo-hydraulic machine at a crosshead speed of 0.1 mm/min resulting in a strain rate on the order of $10^{-4}\,s^{-1}$ in the specimens. Three specimens from each composite were also tested under uniaxial compressive loads at a strain rate on the order of $10^{3}\,s^{-1}$ using a modified split Hopkinson pressure bar (SHPB) with a momentum trap to ensure a single impact on the specimen [25,26]. All the fractured specimens were characterized for their mode of fracture and for identification of microstructural deformation mechanisms using optical microscope and SEM.

For comparison of the constitutive behavior of the composites with their constituents, experiments were also performed on pure W [27], pure Vit105 and Vit106 [21,28]. The pure W was purchased from Alfa Aesar, Ward Hill, MA. It was made by hot rolling powder metallurgical billet without annealing. Pure Vit105 and Vit106 were obtained from the US Army Research Laboratory. The details of the mechanical behavior of these materials were discussed by Li et al. [28] and Jiao et al. [21].

3. Results and discussion

3.1. Morphology

The morphology of the composites was characterized by SEM. Fig. 1a–e shows the micrographs of the polished surfaces of the as received composites. It is seen that all the reinforcing particles (W) are distributed almost uniformly in the amorphous matrix in the first three composites. In Fig. 1c–e, due to the relatively high particle volume fraction (70%), it appears as though the dark amorphous matrix phase is surrounded by the bright W phase. The difference in morphology of the microstructure among the four composites appears to be caused by the different powder size and the processing method used for making the W preforms. In the case of Vit105-W70, a distinctly different morphology is seen (see Fig. 1d and e) compared to others even though it has the same volume fraction as Vit106(LM)-W70 (Fig. 1c). This distinct microstructure is due to the addition of fugitive agent in the W powders, and is possibly because of the different glass (Vit105 instead of Vit106) used. Because the

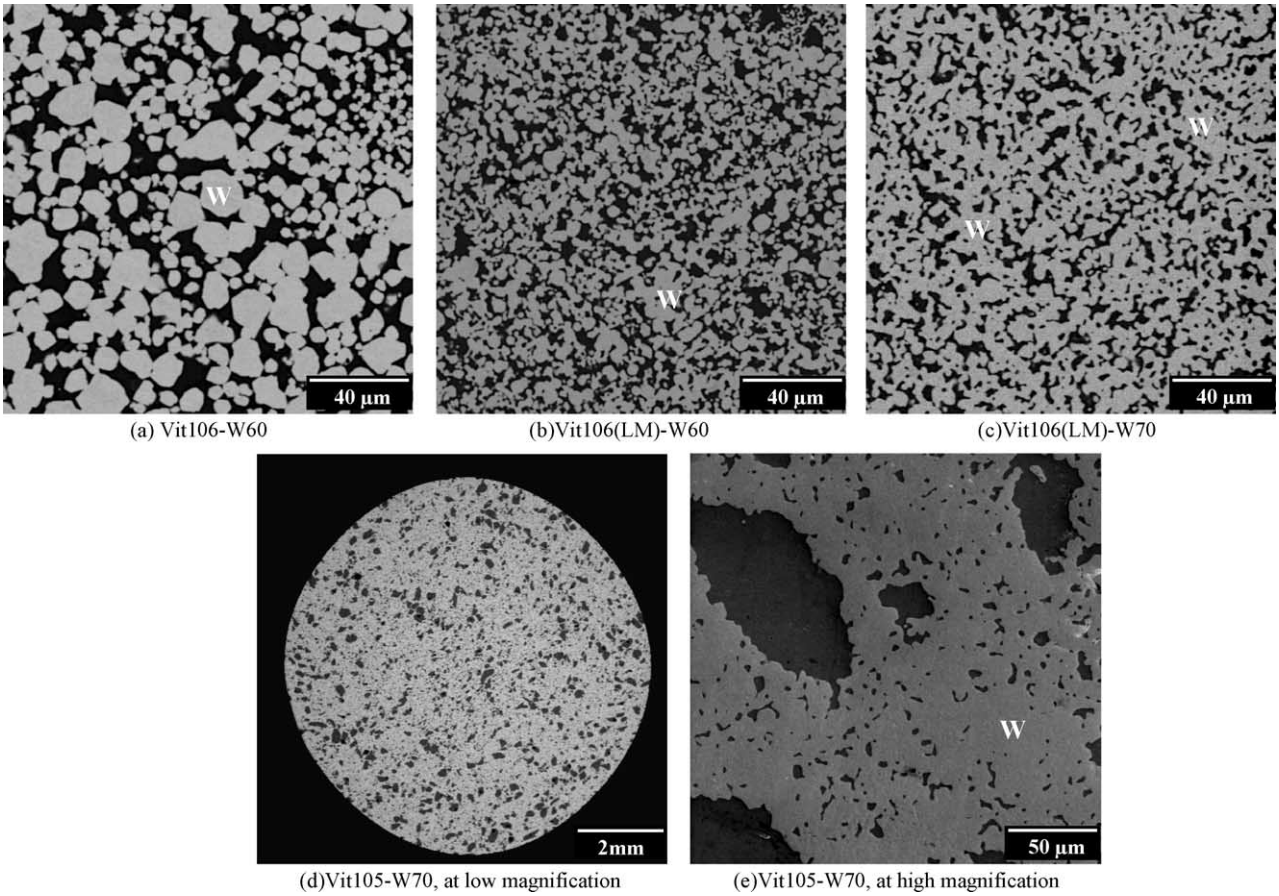

(a) Vit106-W60 (b)Vit106(LM)-W60 (c)Vit106(LM)-W70

(d)Vit105-W70, at low magnification (e)Vit105-W70, at high magnification

Fig. 1. (a–e) SEM micrographs the polished surface of the as received composites.

Table 1
Density and elastic properties of the composites and their components

Material ID	Processing	Density (g/cm^3)		Young's modulus (GPa)		Shear modulus (GPa)		Poisson ratio	
		Measured[a]	ROM[c]	Measured[b]	ROM[c]	Measured[b]	ROM[c]	Measured[b]	ROM[c]
Vit106-W60	CIPping and infiltration	15.20	14.3	230.4	281.3	87.9	108.3	0.32	0.32
Vit106(LM)-W60	CIPping and infiltration	14.30	14.3	221.7	281.3	83.3	108.3	0.33	0.32
Vit106(LM)-W70	CIPping and infiltration	15.67	15.55	269.6	313.7	103.2	121.2	0.30	0.31
Vit105-W70	CIPping and infiltration, resulting in bimodal porosity	15.44	15.53	268.2	313.3	101.1	121.7	0.30	0.31
W		19.3		411		160		0.28	
Vit 106[d]		6.8		86.7		30.8		0.38	
Vit 105[e]		6.73		88.6		32.3		0.37	

[a] From Archimedes' method.
[b] From ultrasonic wave velocity method.
[c] Rule of mixture.
[d] Ref. [19].
[e] Ref. [23].

W preform is continuous and the glass matrix only occupies 30% of the volume, the matrix in this material appears to be dispersed particles. Also, note that there is a bimodal distribution of the matrix material in Vit105-W70. The larger size matrix phase (25–500 μm) is formed by the glass filling up the voids left by the fugitive agent; the smaller size (1–25 μm) matrix phase is formed due to CIPping and sintering of W powders. Except for Vit106-W60, all other composites seem to have a continuous W phase.

3.2. Density and elastic properties

Table 1 shows the results of density and elastic property measurement and the ROM calculations of the composites and their constituents. It is observed that the measured densities for all the composites except for Vit106-W60 agree well with the ROM, which suggests that the porosity in these composites is negligible. For Vit106-W60, the measured density (15.2 g/cm^3) is higher than the calculated value of 14.3 g/cm^3. The higher density suggests that the real volume fraction may be higher than the nominal volume fraction of 60%. The Poisson's ratios by the two approaches are comparable. The measured Young's moduli and shear moduli for all the composites were consistently lower than those estimated by the ROM method. This result is expected because the elastic modulus calculated from the ROM method always provides the upper bound when compared to the experimental results and the values calculated from various micromechanical models [29,30]. The lower value of Young's modulus and shear modulus compared to the ROM method are probably the result of weak interfaces in the composites which affect the measured wave velocities and hence the calculated moduli. Table 1 also shows that the measured and calculated densities as well as the elastic properties of the composites. Note that the values of these properties for Vit106(LM)-W70 and Vit105-W70 are close. This result is probably due to the similar densities (6.8 g/cm^3 for Vit106 and 6.73 g/cm^3 for Vit105) and elastic properties (86.7 GPa versus 88.6 GPa for Young's modulus for Vit106 and Vit105, respectively) for the two different matrices (assuming that the corresponding volume fractions of the constituents in these composites are the same).

3.3. Quasistatic compression

Fig. 2 shows the representative true stress–true strain curves for all the composites under quasistatic compression. For comparison purpose, similar curves for the matrix materials and W are also shown. All the composites exhibit large ductility well over 30% strain, similar to that of the ductile W. However, the pure glass specimens (Vit105 and Vit106) reveal little plastic strains before fracture (less than 2.5%). It is also noted that all the composites and W exhibited a gradual softening behavior after reaching a peak stress level.

From comparison of the true stress–true strain curves of the composites with those of its constituents, it can be inferred that the W reinforcement plays a dominant role in the behavior of the composite due to its large volume fraction. All the composites exhibited a ductility level comparable to that of W. Interestingly, the composites have significantly lower flow stress compared to both the parent materials. The two com-

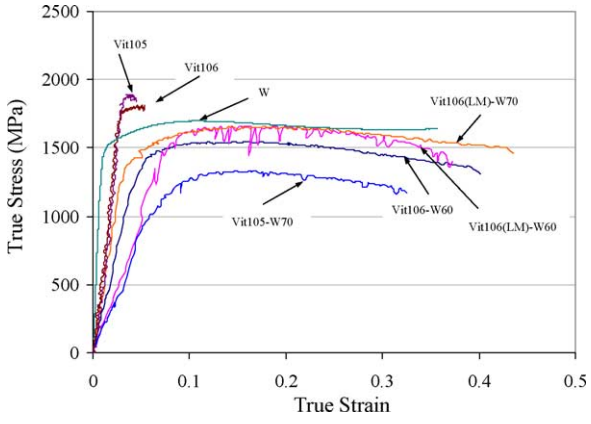

Fig. 2. True stress–true strain curves for composites under quasistatic compression.

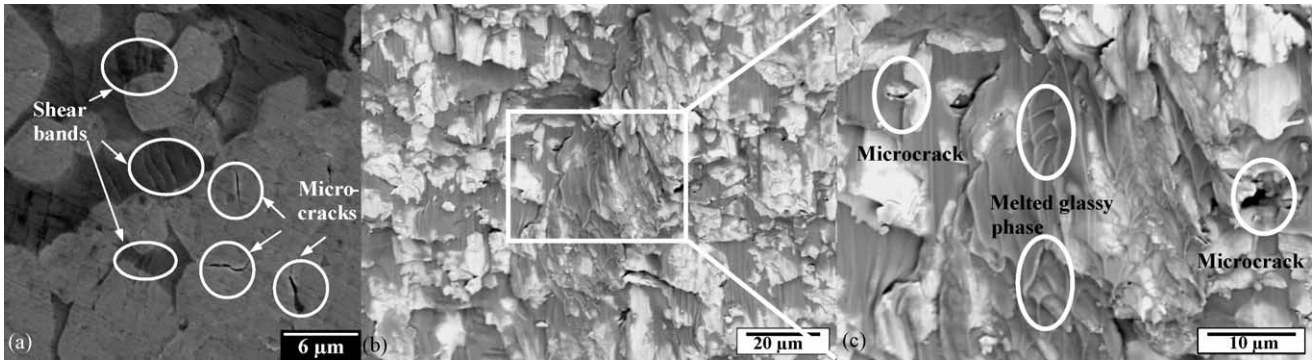

Fig. 3. SEM micrographs of failed specimens for Vit106-W60 after quasistatic compression: (a) polished outer surface revealing shear bands in glassy phase and microcracks in W phase and (b and c) fracture surface revealing melted glassy phase and microcracks.

posites with the LM glass matrix (yttrium used in glass melt) generally exhibited higher flow stress than Vit106-W60 and Vit105-W70. The higher stress is probably due to the continuous W phase in the LM composites, which probably has similar deformation behavior to the pure W, as opposed to discrete W in the latter two composites. Another interesting observation of the behavior is that the composites exhibit higher softening rate than pure W. This behavior is attributed to the induced deformation mechanisms to be discussed in the next section.

From Fig. 2, it is observed that all the Vit106 composites exhibit much larger plastic strain and higher failure stress than Vit105-W70. While Vit106 composites have more uniformly distributed finer W particles, the Vit105-W70 has a bimodal structure which could increase the heterogeneity of the material. Conner et al. [15] found that larger volume fraction (up to 15%) of larger size W particles (up to 150 μm) in Vit106 composite provided the highest strain to failure in quasistatic compression compared to low volume fractions (5 and 10%) and small size (3 and 12 μm) W particulate composites. On the contrary, Choi-Yim et al. [16] noticed in W reinforced Vit106 composites an increased tendency to ductile failure with increased volume fraction and decreasing particle size. Clearly, there seems to be no unanimity on the reinforcement effect of volume fraction and particle size on metallic glasses. It appears that, in addition to volume fraction and particle size, the processing scheme may also strongly influence the mechanical behavior.

3.3.1. *Fracture mode under quasistatic compression*

Under quasistatic compression, most specimens of the Vit106-W60 and Vit106(LM)-W70, and some Vit106(LM)-W60 samples, failed into two similar pieces with fracture angles at around 45°, similar to their glass matrix counterparts [15,17,28]. A loud cracking sound was generally heard followed by a load drop and the separation of the two parts during compression. On the other hand, the Vit105-W70 composite, after the loud noise (which indicates the failure of the specimen), continues to compress into a thin disk with some small fragments separating around the peripheries. This phenomenon was possibly caused by the foamed W preform, which has a continuous W phase with a bimodal size distribution of the glass matrix. The continuity of the ductile W phase provides the possibility for the glass matrix to be confined and squeezed in the W preform and makes the composites more malleable.

Figs. 3–6 shows the SEM micrographs of either the fracture surfaces or the polished sides of the specimens of the Vit106-W60, Vit106(LM)-W60, Vit106(LM)-W70, and Vit105-W70, respectively, after quasistatic loading. In Fig. 3a, numerous shear bands are seen in the metallic glass matrix of Vit106-W60 composite, which suggests that shear

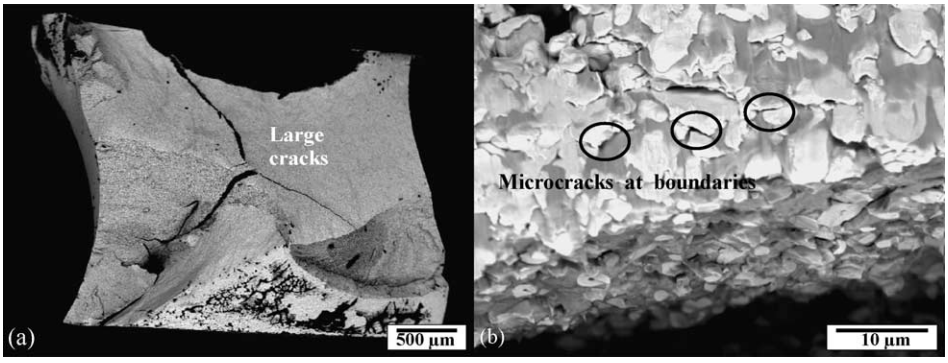

Fig. 4. SEM micrographs of failed specimens for Vit106(LM)-W60 after quasistatic compression: (a) fracture surface with large cracks and (b) microcracks at the phase boundaries and deformed W particles on fracture surface.

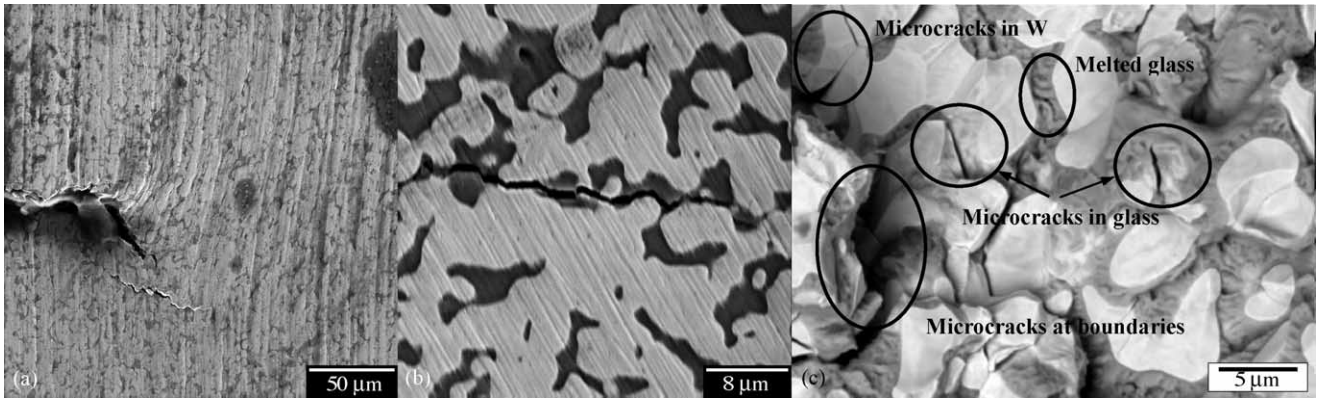

Fig. 5. SEM micrographs of failed specimens for Vit106(LM)-W70 after quasistatic compression: (a) shearbanding at the tip of the crack indicated by offset of surface scratches, (b) polished surface revealing cracks propagating mostly in the glassy phase or along the phase boundaries, and (c) melted glassy phase, microcracks in glass and W particles, and along the boundaries of W and glassy phases on fracture surface.

bands may initiate in the matrix and then develop into cracks. Microcracks are also occasionally seen in the W particles. Fig. 3b and c shows the melted glassy phase and microcracks along the phase boundaries or in the glassy matrix. For Vit106(LM)-W60 composite (Fig. 4a), a distinctive feature is that large cracks (up to 40 μm wide) develop on the fracture surface of the specimens. However, the specimen does not disintegrate into multiple fragments but remains in two large fragments, which suggests that this composite is able to sustain large deformation, probably due to the continuous W preform which is ductile. Although both Vit106-W60 and Vit106(LM)-W60 have the same constituents and volume fractions of reinforcement, their microstructure is considerably different, as seen in Fig. 1a and b. Vit106(LM)-W60 has much finer (average 4–5 μm versus 8 μm) W particles which seem to be continuous on the 2-D SEM micrograph. The finer dispersion of ductile particles leads to higher interfacial area, better homogeneity, improved ductility, and more effective obstruction of crack growth in these composites. Fig. 4b reveals microcracks along the particle boundaries and heavily deformed W particles on the fracture surface in this composite.

Fig. 5a–c shows the micrographs revealing the deformation mechanisms in Vit106(LM)-W70 after quasistatic loading. All the four tested specimens failed into two similar pieces. In Fig. 5a, evidence of shear banding is seen at the tip of the cracks where the polishing scratches have curved. In Fig. 5b, the crack primarily propagates either in the glassy phase or along the boundary of the two phases. On the fracture surfaces, melted glassy phase and microcracks along the boundaries, and occasionally in W particles are seen in Fig. 5c. The above mentioned features were also seen in Vit106(LM)-W60 (Fig. 4b), probably because the only difference between these two materials is the W volume fractions.

Fig. 6a and b shows the micrographs of polished surfaces of Vit105-W70 after quasistatic loading. Recall that this composite has bimodal distribution of glassy phase (grey regions in Fig. 1), which is surrounded by the continuous W phase. Upon loading, microcracks develop in the glassy

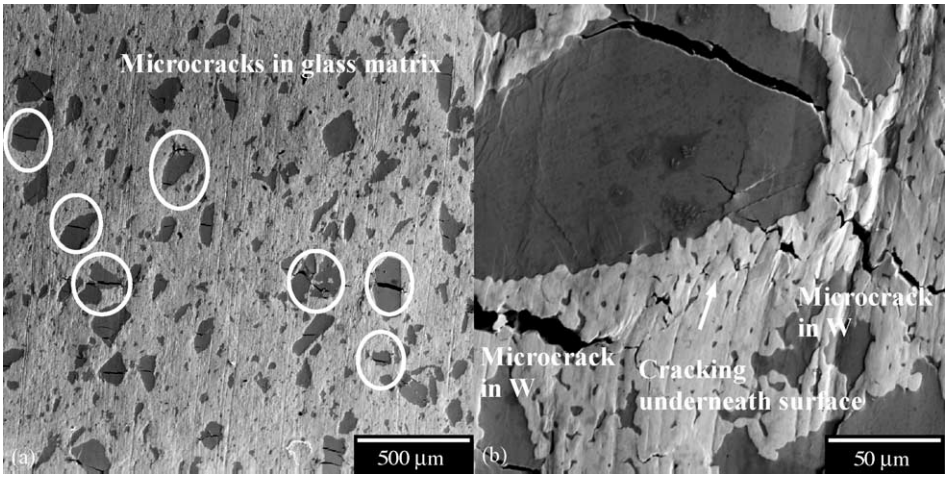

Fig. 6. SEM micrographs of failed specimens for Vit105-W70 after quasistatic compression: (a) polished surface revealing micro-cracks mostly in glass and (b) microcracks in the composite due to shear as indicated by offset of polishing scratches.

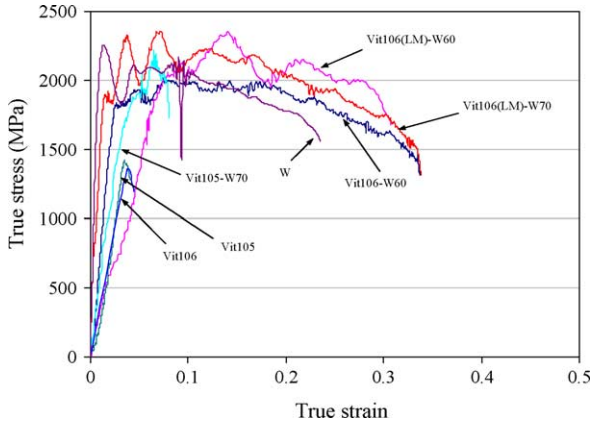

Fig. 7. True stress–true strain curves for composites under dynamic compression.

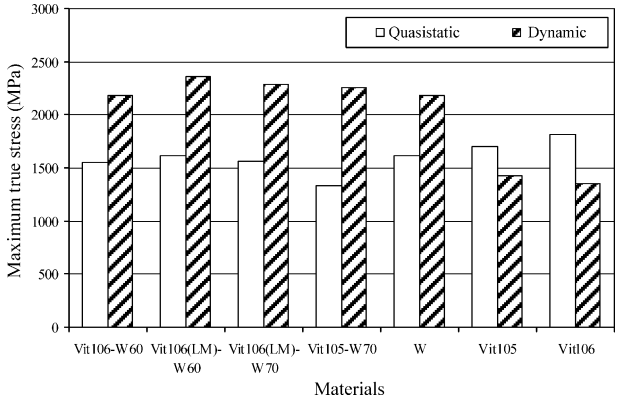

Fig. 8. Average maximum true stress of the composites and the constituents.

phase as well as in the W phase, as seen in the above figures.

In general, it is seen in all the composites that cracks are mostly along the phase boundaries, with occasional shear bands and cracks in the glassy phase. Conner et al. [15], Hays et al. [4], and Jiao et al. [21] observed similar failure mechanisms in metallic glass composites. They noted that shear bands initiated in the glass matrix and when they reach the W reinforcement, they either propagate through the W phase or diverge at the interfaces. Some of the shear bands develop into cracks. This phenomenon of shear banding and microcracking throughout the specimen leads to increased plasticity of the composites. These observations are verified in our micrographs.

3.4. Dynamic compression

Fig. 7 shows the representative true stress–true strain curves for composites under dynamic compressive loading at a nominal strain rate of around 4000 s^{-1}. Similar to quasistatic compressive behavior, all the composites behave in a manner close to that of W under dynamic compression. As the plastic deformation progresses, all the composites reach a maximum stress and then show a gradual softening behavior. Plastic strains well in excess of 30% are observed.

Compared to quasistatic loading, the yield stress of all the composites is significantly greater under dynamic loading. This positive rate sensitivity of the yield stress (i.e., increase in yield and flow stresses at higher strain rates) can be attributed to the higher volume fraction of the W reinforcement. Both W and W-composites are well known to exhibit an increase in strength with increase in strain rate [31–33] and accordingly the composites behavior seems to be dominated by the W behavior.

While the above composites exhibit positive rate sensitivity, note from Figs. 2 and 7 that the pure BMGs (Vit105 and Vit106) exhibit a negative rate sensitivity, i.e., decrease in yield stress with increase in strain rate. This negative rate sensitivity of compressive fracture strength of BMGs was earlier investigated by the same authors [28] and rationalized as follows. In pure BMGs (i.e., Vit105), shear bands initiate well below the yield stress and grow to maturity upon continued loading during quasistatic deformation. Whereas under dynamic loading, due to the available excess energy, cracks initiate immediately upon shear band initiation and cause fracture of the specimen. Thus, a lower fracture stress is seen under dynamic loading which results in negative rate sensitivity for pure BMGs.

Fig. 8 shows the comparison of average maximum true stress for the composites and the constituents from quasistatic and dynamic compressive loading. It is obvious that for all the

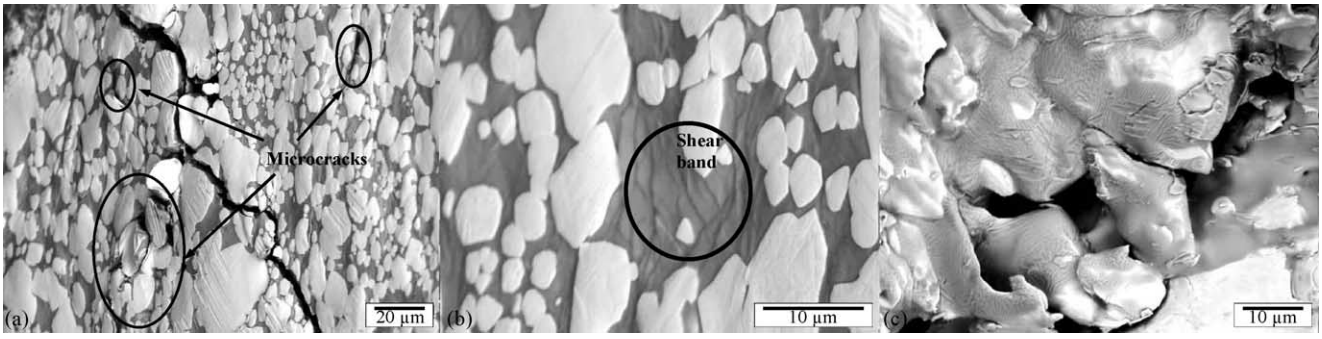

Fig. 9. SEM micrographs of failed specimens for Vit106-W60 after dynamic compression: (a) polished outer surface revealing crack propagation mostly along the particle boundaries, (b) shear bands in the glassy phase and severely deformed W particles, and (c) melted glassy phase and voids on fracture surface.

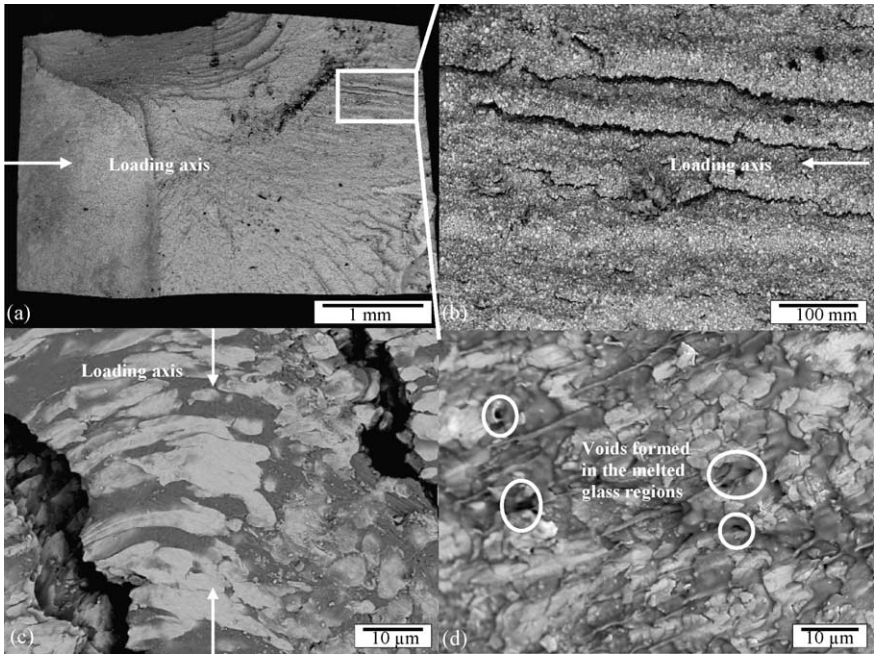

Fig. 10. SEM micrographs of failed specimens for Vit106(LM)-W60 after dynamic compression: (a) fracture surface with several cracks, (b) magnified view of cracks on the fracture surface, and (c) severely deformed W particles on the fracture surface.

composites, the maximum stress under dynamic compression is higher than that under quasistatic compression; while for BMGs, the converse is true, i.e., Vit105 and Vit106 have lower maximum strength at higher strain rates [21,28].

3.4.1. Fracture mode under dynamic compression

During dynamic compression, it is observed that, except for Vit106-W60 where the specimens failed into two pieces at approximately 45° to the loading axis, all specimens of the other three composites failed into multiple fragments under dynamic compression. Figs. 9–12 shows the SEM micrographs of the fractured surfaces or polished sides of the samples of the dynamically loaded specimens for all the composites. The deformation and fracture features shown in these micrographs (i.e., cracks along the phase boundaries, melted glass, and deformation of W particles) for all the four composites are similar to those under quasistatic compression. As expected, the severity of the melting of glass and the deformation of W particles is greater due to adiabatic conditions that exist during the dynamic loading and the subsequent high temperature rise. Except for Vit105-W70, which is compressed into thin disks under quasistatic loading and thus has no observable fracture surface, all the fracture surfaces of the composite specimens that are dynamically loaded are more rugged and have more deformation-induced defects than their quasistatic counterparts.

Numerous microcracks are seen on the fracture surfaces of Vit106-W60 (Fig. 9a). Cracks propagate mostly along the particle boundaries. Shear bands in the glass matrix and heavily deformed W particles are seen in the micrographs of Fig. 9a–c. Fig. 10 reveals the fracture surface of Vit106(LM)-W60. In contrast to the quasistatically com-

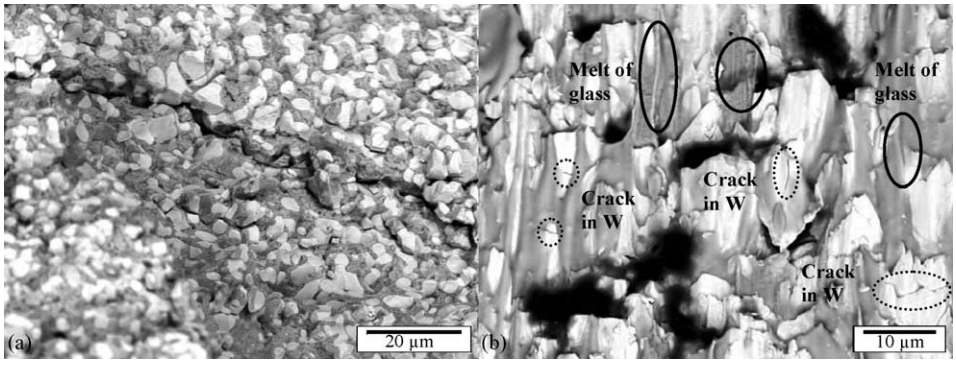

Fig. 11. SEM micrographs of failed specimens for Vit106(LM)-W70 after dynamic compression: (a) fracture surface revealing crack propagating along phase boundaries and (b) melted glassy phase, and deformed and cracked W particles on fracture surface.

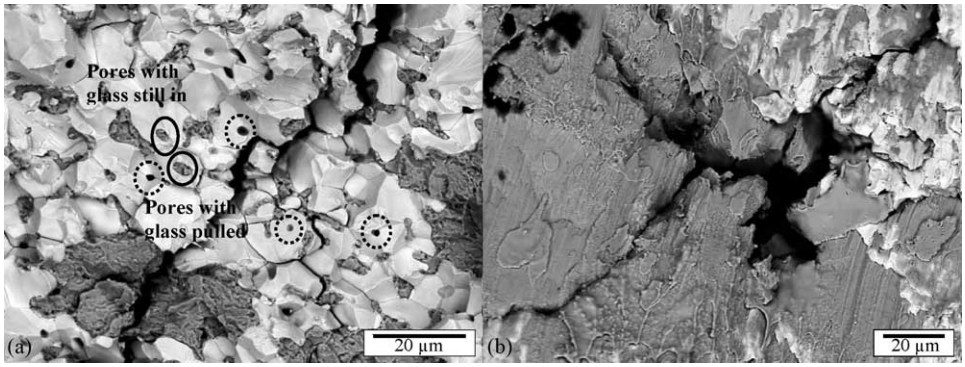

Fig. 12. SEM micrographs of failed specimens for Vit105-W70 after dynamic compression: (a) fracture surface revealing poorly distributed matrix and reinforcement, (b) cracks on fractured surface propagating along phase boundaries, small pores left after glass was pulled out and small pore with residue glass phase, and (c) melted glassy phase and cracks on fracture surface.

pressed counterparts, the micrographs of fracture surface in Fig. 10b shows multiple cracks parallel to the loading axis. Fig. 10c shows a magnified view of the area between two of the cracks. It is seen that the W particles are severely deformed/compressed during deformation. Fig. 10d shows severely melted glassy phase and void formation on the fracture surface of Vit106(LM)-W60, which is a result of high temperature rise during dynamic loading. Fig. 11a and b reveal fracture surfaces of Vit106(LM)-W70. It appears to fail in a manner similar to Vit106(LM)-W60 with cracking along the phase boundaries, melted glassy phase and severely deformed W particles. Note that Vit106(LM)-W70 has only slightly larger particle sizes than Vit106(LM)-W60 (see Fig. 1a and b), therefore, the above mentioned similarities in fracture mode between these two composites appear to be reasonable.

The specimens of Vit105-W70 (see Fig. 12a and b) all fractured into multiple fragments. Fig. 12 shows cracks propagating along the W phase boundaries. Smaller pores depleted of glassy phase or filled with residual glassy phase are also seen. It appears as if the glass initially filling the pores failed in a brittle manner or simply got pulled out upon loading. This behavior suggests a weak bond between the glass and W phases resulting in the lowest failure stress and failure strain among all the four composites. Melted glass, microcracks in the glassy phase or at the phase boundaries, and deformed W particles are shown in Fig. 12b, which are the common features on the fracture surfaces of all the composites.

Finally, a note of caution is necessary while making comparison between the behavior of W and the composites. The W phase in the composite has undergone various steps during processing of the composite (CIPping, sintering for preform, subjected to pressure and temperature again during melt infiltration, etc.), and therefore the true stress–true strain curve obtained from a commercial pure W (not annealed) can only provide an approximate guideline to the mechanical behavior of W phase in this composite. Nevertheless, it is obvious that the high volume fraction of W in these composites dominates the constitutive behavior and hence all the composites exhibit high strain rate sensitivity of fracture strength.

4. Conclusions

- The W particle reinforced Vit106 and Vit105 composites exhibited large ductility under both quasistatic and dynamic compressive loading. The behavior is mainly attributed to the large volume fraction of W, which exhibits high ductility.
- The yield stress and the maximum stresses are higher for all the composites under dynamic compression than under quasistatic compression. This positive rate sensitivity of fracture strength is also attributed to the large volume fraction of W, which is known to be highly rate sensitive.
- Processing method strongly influences the resulting microstructure, and thus the mechanical behavior of the composites even when they have the same matrix, reinforcement type, and volume fractions.
- In general, the deformation behavior is dominated by shear banding in the glassy phase, cracking along the particle boundaries, and severe deformation of W particles.

Acknowledgements

This research is supported by the Weapons and Materials Research Directorate, US Army Research Laboratory, Aberdeen Proving Ground, MD, under the contract no. DAAD19-01-1-0492 through US Army Robert Morris Acquisition Center.

References

[1] C.C. Hays, W.L. Johnson, Presented at ISMANAM-99, Dresden, Germany, August 30–September 3, 1999.
[2] R. Doglione, S. Spriano, L. Battezzati, Nanostruct. Mater. 8 (1997) 447–456.
[3] C. Fan, C. Li, A. Inoue, V. Haas, Phys. Rev. B 61 (2000) 3761–3763.
[4] C.C. Hays, C.P. Kim, W.L. Johnson, Phys. Rev. Lett. 84 (2000) 2901–2904.
[5] U. Kuhn, J. Eckert, N. Mattern, L. Schultz, Appl. Phys. Lett. 80 (2002) 2478–2480.

[6] H. Choi-Yim, R. Busch, U. Koster, W.L. Johnson, Acta Metall. 47 (1999) 2455–2462.
[7] R.B. Dandliker, R.D. Conner, W.L. Johnson, J. Mater. Res. 13 (1998) 2896–2901.
[8] J. Eckert, M. Seidel, A. Kubler, U. Klement, L. Schultz, Scripta Mater. 38 (1998) 595–602.
[9] C. Moel1e, I.R. Lu, A. Sagel, R.K. Wunderlich, J.H. Perepezko, H.J. Fecht, Mater. Sci. Forum (1998) 269–272.
[10] S. Deledda, J. Eckert, L. Schultz, Scripta Mater. 46 (2002) 31–35.
[11] M. Calin, J. Eckert, L. Schultz, Scripta Mater. 48 (2003) 653–658.
[12] Y.C. Kim, J.H. Na, J.M. Park, D.H. Kim, J.K. Lee, W.T. Kim, Appl. Phys. Lett. 83 (2003) 3093–3095.
[13] H. Choi-Yim, W.L. Johnson, Appl. Phys. Lett. 71 (1997) 3808–3810.
[14] X.H. Lin, W.L. Johnson, J. Appl. Phys. 78 (1995) 6514–6519.
[15] R.D. Conner, H. Choi-Yim, W.L. Johnson, J. Mater. Res. 14 (1999) 3292–3297.
[16] H. Choi-Yim, R.D. Conner, W.L. Johnson, Mater. Sci. Forum 360–362 (2001) 55–60.
[17] H. Choi-Yim, R.D. Conner, F. Szuecs, W.L. Johnson, Scripta Mater. 45 (2001) 1039–1045.
[18] H. Choi-Yim, J. Schroers, W.L. Johnson, Appl. Phys. Lett. 80 (2002) 1906–1908.
[19] H. Choi-Yim, R.D. Conner, F. Szuecs, W.L. Johnson, Acta Mater. 50 (2002) 2737–2745.
[20] X. Gu, T. Jiao, L.J. Kecskes, R.H. Woodman, C. Fan, K.T. Ramesh, T.C. Hufnagel, J. Non-Cryst. Solids 317 (2003) 112–117.
[21] T. Jiao, L.J. Kecskes, T.C. Hufnagel, K.T. Ramesh, Metall. Mater. Trans. A 35A (2004) 3439–3444.
[22] Z. Bain, G. He, G.L. Chen, Scripta Mater. 46 (2002) 407–412.
[23] Z. Bian, M.X. Pan, Y. Zhang, W.H. Wang, Appl. Phys. Lett. 81 (2002) 4739–4741.
[24] Z. Bian, R.J. Wang, D.Q. Zhao, M.X. Pan, Z.X. Wang, W.H. Wang, Appl. Phys. Lett. 82 (2003) 2790–2792.
[25] S. Nemat-Nasser, J.B. Isaacs, J.E. Starrett, Proc. R. Soc. London A 435 (1991) 371–391.
[26] G. Subhash, G. Ravichandran, ASM Handbook, Mechanical Testing and Evaluation, vol. 8, ASM International, 2000, pp. 497–504.
[27] Q. Wei, K.T. Ramesh, E. Ma, L.J. Kesckes, R.J. Dowding, V.U. Kazykhanov, R.Z. Valiev, Appl. Phys. Lett. 86 (2005) 101907-1–101907-3.
[28] H. Li, G. Subhash, X.-L. Gao, L.J. Kecskes, R.J. Dowding, Scripta Mater. 49 (2003) 1087–1092.
[29] W.D. Callister, Materials Science and Engineering: An Introduction, third ed., John Wiley & Sons, 1994, pp. 161–162, 525.
[30] R.M. Jones, Mechanics of composite materials, second ed., Taylor & Francis, Philadelphia, PA, 1999, pp. 137–145.
[31] S. Yadav, K.T. Ramesh, Mater. Sci. Eng. A A203 (1995) 140–153.
[32] G. Subhash, Y.J. Lee, G. Ravichandran, Acta Metall. 42 (1994) 319–330.
[33] G. Subhash, Y.J. Lee, G. Ravichandran, Acta Metall. 42 (1994) 331–340.